VNU Journal of Science: Mathematics - Physics

Journal homepage: https://js.vnu.edu.vn/MaP

Original Article

Characterization and Microwave Absorption Properties of Lead-Free $Bi_{0.5}(Na_{0.80}K_{0.20})_{0.5}TiO_3$ Synthesized by Sol-Gel Method

Nguyen Dang Co[1], Tran Duc Huy[1], Bui Thi Thu Thuy[1], Nguyen Thi Luong[1], Dong Quoc Viet[1], Le Viet Cuong[1], Dang Duc Dung[2], Ngo Duc Quan[2], Tran Mau Danh[1], Pham Duc Thang[3], Bui Dinh Tu[1,*]

[1]*VNU University of Engineering and Technology, 144 Xuan Thuy, Cau Giay, Hanoi, Vietnam*

[2]*Hanoi University of Science and Technology, No.1 Dai Co Viet, Hanoi, Vietnam*

[3]*Phenikaa University Nano Institute, Phenikaa University, Nguyen Trac, Ha Dong, Hanoi, Vietnam*

Received 27 July 2021
Revised 14 September 2021; Accepted 18 September 2021

Abstract: Lead-free $Bi_{0.5}(Na_{0.80}K_{0.20})_{0.5}TiO_3$ (BNKT) particles were synthesized by using sol-gel method. The samples were investigated by X-ray diffractometry (XRD), scanning electron microscope (SEM), energy-dispersive X-ray spectroscopy (EDX), and vibrating sample magnetometer (VSM). The absorption of microwaves of the lead-free BNKT powders is determined from the magnetic (permeability) and dielectric (permittivity) properties at the frequency range from 2 to 18 GHz. Absorption characteristics of paraffin(wax)-mixed BNKT compounds at different sample thicknesses were also investigated. The microwave absorption properties show that the maximum reflection loss is -21.72 dB (99.9%) at 13.66 GHz with a thickness of 3.2 mm. BNKT composites are thought to be used as a promising microwave absorption material.

Keywords: BNKT, microwave absorption, reflection loss, sol-gel.

1. Introduction

The fact that electromagnetic wave pollution is increasing day by day has become an extremely urgent problem [1]. The absorption of electromagnetic waves has emerged as a novel field of

* Corresponding author.
E-mail address: buidinhtu@vnu.edu.vn

https//doi.org/10.25073/2588-1124/vnumap.4665

applications where microscopic nanomaterials with their intrinsic dielectric and magnetic properties can be used to solve the above mentioned problem [2, 3].

Recently, microwave absorbing materials have received a lot of attention because of increasing telecommunication, military and commercial applications in reducing radar cross-section in the gigahertz frequency band for stealth technology purposes, electromagnetic shielding [4]. Electromagnetic microwave absorption efficiency is related to parameters such as dielectric constant, permeability, impedance matching, the microstructure of the absorber [5]. This is mainly determined by the properties of the absorbent about the type of material used [6, 7]. Materials with the high dielectric constants such as ceramics, metals, ionic fillers can be used for making microwave-absorbing materials. Among the dielectric filling candidates for microwave absorption, particles of lead-free $Bi_{0.5}(Na,K)_{0.5}TiO_3$ (BNKT) with perovskite structure are particularly interesting.

BNKT or (1-x)BNT-xBKT is a compound of $(Bi_{0.5}K_x)TiO_3$ (BKT) of tetragonal structure incorporated with $(Bi_{0.5}Na_{1-x})TiO_3$ (BNT) of rhombohedral structure. The advantages of the BNKT ceramic consist of the high Curie temperature, good dielectric and piezoelectric properties at $0.16 \leq x \leq 0.20$ [8]. The excellent electrical properties of (1-x)BNT-xBKT ceramics are always observed for their composition near a morphotropic phase boundary (MPB) between rhombohedral-tetragonal phases [9-11]. The dielectric, piezoelectric, and electromechanical properties are sharply enhanced at this boundary. Many studies have shown that, at the optimal composition $Bi_{0.5}(Na_{0.8}K_{0.2})_{0.5}TiO_3$ with rhombohedral-tetrahedral (MPB) phase boundary, these materials possess both the high relative permittivity, and good ferroelectric properties [12-14]. The maximum dielectric constant (ε_r = 1030) was obtained at the composition of x = 0.20 [10, 15]. However, most of the studies only showed the ferroelectric and piezoelectric properties of BNKT materials without any research or specific indication of their electromagnetic wave absorption properties.

In addition, paraffin wax is an excellent insulator, with a resistivity ranging from 10^{13} to 10^{17} Ω.m [16]. This is better than almost any other material except some plastics, f. i. teflon. Paraffin wax is often used as substrates in electronic devices due to its good dielectric properties. It is also widely used for microwave absorption and electrical shielding [17-19].

In this present work, lead-free BNKT filler was prepared by sol-gel method. The microwave absorption properties of BNKT/paraffin wax composites with a BNKT/paraffin wax weight ratio of 50:50 were investigated at the sample thicknesses ranging from 1.6 to 4.0 mm, in the frequency range from 2 to 18 GHz.

2. Experimental

2.1. Material

All chemicals used have the analytical grade as purchased without further purification. The lead-free $Bi_{0.5}(Na_{0.80}K_{0.20})_{0.5}TiO_3$ particles were synthesized through the sol-gel process described in [12, 13, 20]. To obtain the desired phase, sodium nitrate ($NaNO_3$, ≥ 99%, Sigma-Aldrich), potassium nitrate (KNO_3, ≥ 99%, Sigma-Aldrich), bismuth nitrate ($Bi(NO_3)_3.5H_2O$, ≥ 98%, Sigma-Aldrich), and titanium isopropoxide ($C_{12}H_{28}O_4Ti$, ≥ 99%, Sigma-Aldrich) were used. Acetic acid (CH_3COOH) and acetylaxetol ($C_5H_8O_2$) were chosen as cosolvents. Afterward, 9 mol.% excess amount of potassium nitrate and 11 mol.% excess amount of sodium nitrate were added to compensate their possible loss during the high-temperature annealing [20].

2.2. Synthesis of BNKT Particulates

The synthesis of BNKT powders consists of six steps (Figure 1). First, the acetates and the nitrates were dissolved separately in glacial acetic acid (1). Secondly, titanium isopropoxide was dissolved in a solution of acetylaxetol (2), in which nitrate solution was slowly added. The colour change occurred in the aqueous phase from white to yellow. In the third stage, after five hours of continuous stirring at 70 ºC (3). The mixture was heated at 80 °C for 24 hours and dried in a vacuum oven (4). Finally, the sample was calcined at 700 °C for 60 min (5) before being grinded in a mortar for 2 hours (6). The heating rate for the annealing process was 5 °C/min under normal conditions.

Figure 1. The six-step preparation scheme for BNKT powders by sol-gel method.

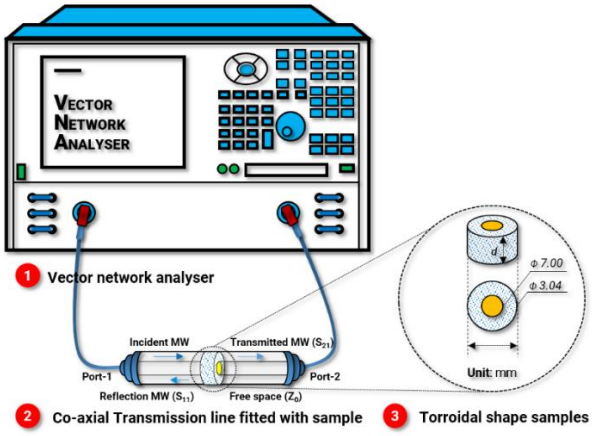

Figure 2. Sample preparation and experimental design of electromagnetic wave absorption measurement: Vector network analyser (1); Co-axial transmission line fitted with sample (2); and Torroidal shape samples (3).

2.3. Characterization

The crystalline data of the sample was collected on X-ray diffractometer (XRD) (Bruker D5005 Diffractometer) using Cu Kα irradiation (λ = 1.5406 Å, 40.0 kV, 40.0 mA). Size-distribution, morphology, and surface composition of power was characterized by a scanning electron microscope (SEM) on a Hitachi S-4800 equipped with an energy-dispersive X-ray analysis (EDX). The magnetic

hysteresis loops were measured using a vibration magnetometer (VSM, Lakeshore 7404) at 292 K and under a 5 kOe magnetic field. The hysteresis loops of the polarization electric field (P E) were measured at applied voltages ranging from -150 V to 150 V. Frequency of 1000 Hz using a Precision LC II ferroelectric test system from Sawyer Tower (Radiant Technologies. Inc). The temperature dependence of dielectric properties was investigated over the frequency range from 1 kHz to 4 MHz using an LCR meter (TEGAM, PM3550).

The electromagnetic wave absorption properties of samples were measured by using a vector network analyzer (VNA, MS4644A, Anritsu, Atsugi) in 2-18 GHz. The coaxial samples were prepared with the paraffin wax matrix (mass ratio, 1:1). The dimension of coaxial rings was ϕ = 7.0 mm in outer diameter and ϕ = 3.05 mm in inner diameter (Figure 2). Based on the transmission line theory, the reflection loss (RL) was calculated according to the following equations (1-2) [21]:

$$\boldsymbol{RL} = 20\log_{10}\left|\frac{Z_{in}-1}{Z_{in}+1}\right| \quad (1)$$

$$\boldsymbol{Z_{in}} = \sqrt{\frac{\mu_r}{\varepsilon_r}}\tanh\left[j\frac{2\pi f d}{c}\sqrt{\mu_r\,\varepsilon_r}\right] \quad (2)$$

where Z_{in}, μ_r and ε_r are the normalized input impedance, permittivity, and permeability of the sample, respectively. The *f*, *d*, and *c* represent electromagnetic wave frequency, thickness (*m*) of sample, and velocity of the electromagnetic wave in vacuum, respectively.

3. Results and Discussion

Figure 3 showed XRD patterns with a few characteristic peaks for planes such as (100), (110), (111), (200), (210), (211), (220), and (310) of BNKT powder calcined at 700 °C in 1 hour where 2θ = 20 - 80°. It can be seen that the sample exhibited a single perovskite structure with a high purity. The XRD patterns of BNKT contained no secondary phases (or impurity peaks) according to the detection limit of the equipment, which is consistent with the results that have ever been reported by Camargo et al. [12] and Chen et al. [13]. The symmetry of the powder sample was characterized as rhombohedral (see peak $(200)_R$ at $2\theta \approx 46.701$ of Figure 3) [22].

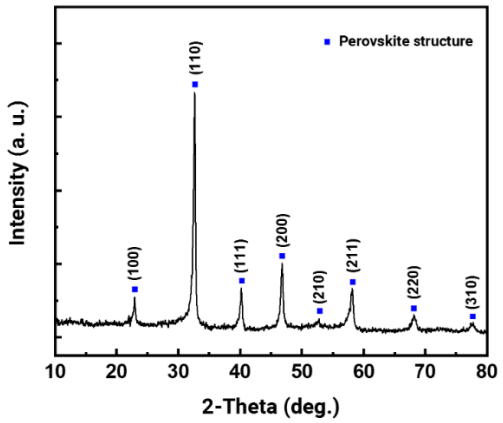

Figure 3. XRD patterns of BNKT powders sintered at 700 °C in 1 hour at 2θ range of 20 - 80°.

Figure 4a is the microstructure SEM image of the BNKT powder samples sintered at 700 ºC for 1 hour. The results show that the particles exist in the form of clusters of a size up to several hundred nanomet. Meanwhile, the average size of BNKT particles is 80-100 nm. The small particles have a defined size in the range of 25-30 nm. Meanwhile, there are still larger particles with the size from 0.2 to 0.4 μm. This is explained by the BNKT grinding process, the particle dispersion and impact forces are not uniform. The clustering of the particles is thought to be at the nanometer size, a large surface area to volume ratio, thus making the binding energy on the surface large. Accordingly, the Van der Waals attraction and electrostatic interactions that exist between particles tend to cause the particles to clump and clump together.

Figure 4b is the EDX spectra of a BNKT sample. The inset of the figure shows the surface morphology of the selected area for EDX measurement. The EDX spectra reveal a pure compound of $Bi_{0.5}(Na_{0.80}K_{0.20})_{0.5}TiO_3$ which show all expected elements, such as Bi, Na, K, Ti, and O elements in the composite. These elements are compatible with the precursor elements, as indicated in Figure 4b.

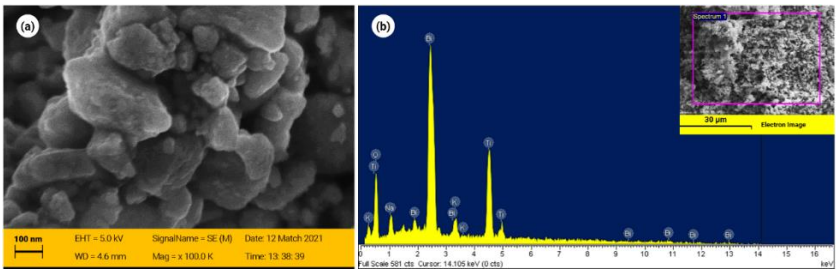

Figure 4. SEM images of pure BNKT powder sintered at 700 ºC in 1 hour (a); EDX spectra of pure $Bi_{0.5}(Na_{0.80}K_{0.20})_{0.5}TiO_3$, the inset in figure shows the selected area of samples for chemical analysis (b).

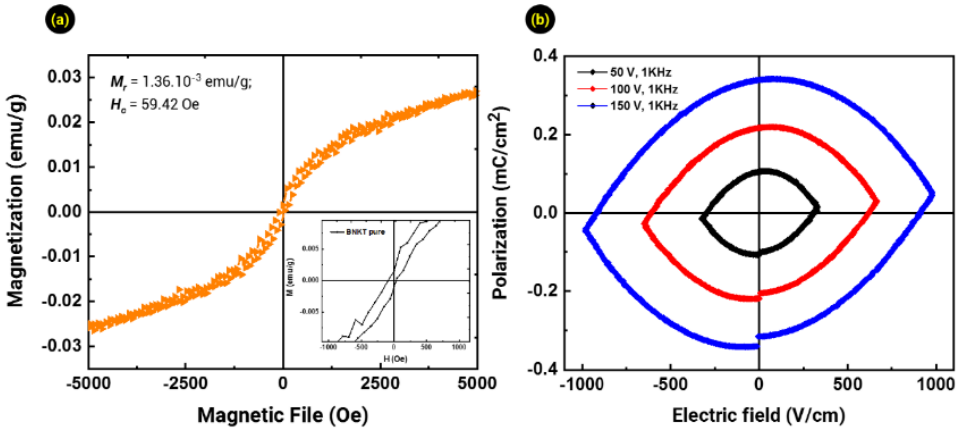

Figure 5. Hysteresis loop of pure BNKT powder measured at room temperature; the inset shows the expanded low-field region (a); P-E ferroelectric hysteresis line of BNKT powder sample at room temperature with a voltage applied between -150 V and 150 V and a frequency of 1kHz (b).

Magnetic properties of a sample are strongly influenced by many its parameters such as crystallinity, particle size, shape, and density of crystalline defects. Figure 5a presents the hysteresis curve of the BNKT powder sample at room temperature for an external magnetic field of 5 KOe. It can be seen that the sample exhibits a characteristic hysteresis curve for weak ferromagnetic materials with intrinsic

magnetic properties including low saturation magnetization (M_s); residual magnetization (M_r); and the coercive field (H_c) is close to zero. The BNKT powder sample with an external magnetic field of 5 kOe with H_c = 59.42 Oe; M_s, M_r values were found to be $26.70.10^{-3}$ emu/g and $1.36.10^{-3}$ emu/g, respectively. The cause of the weak ferromagnetic properties of BNKT materials can be attributed to the contribution of the Ti^{4+} component. Although the magnetic property is weak, it has contributed to the enhancement of the permeability of the BNKT composite material mixed with the paraffin wax, thereby further the electromagnetic wave absorption efficiency can be improved.

To investigate the ferroelectric properties of BNKT ceramics sintered at 700 °C for 1 hour, the hysteresis loops were performed with a voltage applied between -150 V and 150 V and a frequency of 1 kHz (Figure 5b). The graph shows that the ceramic sample has a typical ferroelectric hysteresis pattern. The remnant polarization P_r and coercive electric field E_c of the systems at different voltages are determined and given in Table 1.

Table 1. Remnant polarization and coercive electric field of BNKT ceramics at different voltages

U (V)	**50**	**100**	**150**
E (kV/cm)	0.33	0.67	1
$\boldsymbol{P_r}$ (μC/cm^2)	0.106	0.217	0.34
$\boldsymbol{E_c}$ (V/cm)	308	619	910

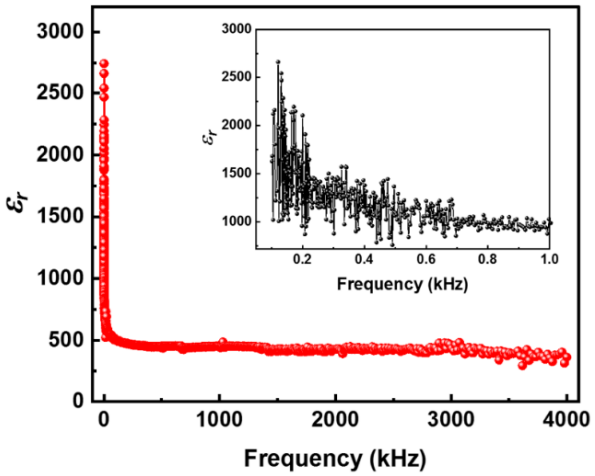

Figure 6. The dielectric constant ε_r of the materials of BNKT ceramics at room temperature in the frequency range 100 Hz to 4 MHz, the inset shows the expanded low- frequency region.

The dependence of the dielectric constant ε_r over f, with the frequency range from 100 Hz to 4 MHz at room temperature BNKT ceramic is illustrated inFigure 6. This is the results of the investigation of palletized BNKT materials with a diameter of 5.52 mm and a thickness of 1.5 mm. Figure 6 demonstrates a clear influence of the dielectric constant on the frequency. In the low-frequency range from 100 Hz to 1 kHz, the dielectric constant of the sample reaches a large value, but decreases sharply with increasing frequency. Largest dielectric constant value is of 2663 at 121 Hz, and decreases to 990 (namely in 2.69 times) at the frequency of 1 kHz. For large frequency ranges from 10 kHz to 4 MHz, the dielectric constant value tends to decrease gradually. The dielectric constant value of the BNKT ceramic sample at 10 kHz, 100 kHz and 1 MHz is of 653, 508 and 451, respectively. The lowest dielectric constant measured at 4 MHz is 362.

Figure 7 illustrates the real and imaginary parts of the complex permeability and complex permeability of BNKT/paraffin with the mass ratio of 50%, thickness of 3.2 mm) as a function of the microwave frequency. It can be seen that the real part (ε'), imaginary part (ε'') of the permittivity and real part (μ'), imaginary part (μ'') of the permeability of composites are relatively small and almost unchanged over the entire frequency range from 2 to 12.5 GHz and from 14.5 to 18 GHz. In the frequency range of 13.66 GHz they showed a clear change in value.

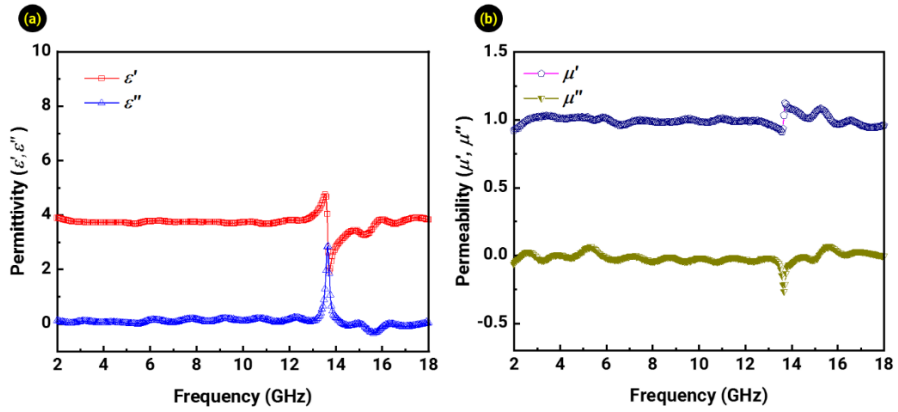

Figure 7. The real (ε') and imaginary (ε'') part of complex permittivity (a);
The real (μ') and imaginary part (μ'') part of complex permeability (b) of BNKT/paraffin wax measured in the 2–18 GHz frequency interval.

In Figure 7a, the real values for parts (ε') of BNKT/paraffin are almost unchanged at 3.75 in the 2-12 GHz frequency range. Then a sharp peak appearedachieved at 4.76 to 13.34 GHz, dropped to 1.98, then gradualy rised to 3.83 at 18 GHz. In addition, the values of the imaginary part (ε') are very small, approximately zero in the entire frequency range, and have a single peak of 2.85 at 13.66 GHz.

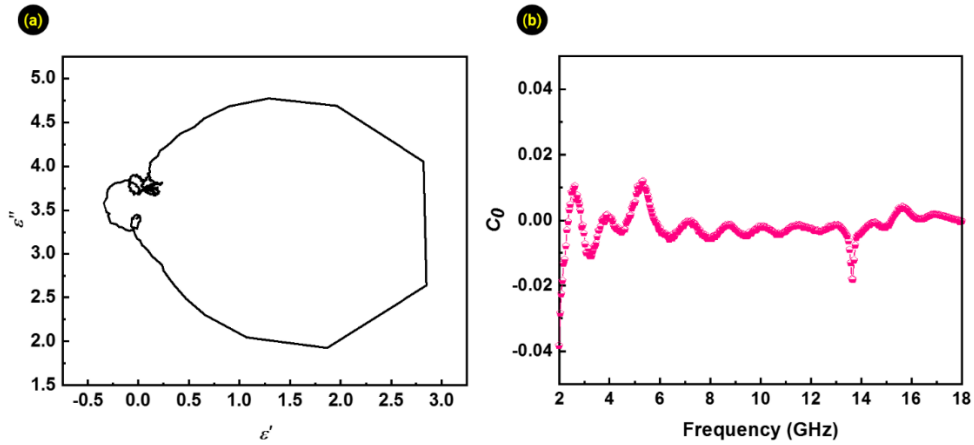

Figure 8. The typical Cole semicircular curve (a); and the C_0 value (b) of BNKT/paraffin wax measured in the 2–18 GHz frequency interval.

Similar to the real part (ε') of the permittivity, the values of the real part of the permeability (μ') of the BNKT/paraffin wax composites have a small change from 1.03 to 0.90 in the frequency range from 2 to 13.6 GHz (Figure 7b). The value of (μ') represents a unique peak of 1.13 at 13.66 GHz and a smaller peak of 1.1 at 15.25 GHz, then gradually decreases and reaches a value of 0.95 at 18 GHz. The imaginary part (μ'') values are very small, close to zero, and vary continuously throughout the frequency range, also having a minimum (- 0.27) at 13.66 GHz. Thus, it can be concluded that the cures of ε', ε'', μ' and μ'' appear with maximum and minimum peaks at 13.66 GHz, which can directly affect the dielectric as well as magnetic loss in BNKT/ paraffin wax materials.

The curve of ε' versus ε'' is a single semicircle, which is generally called the Cole–Cole semicircle. Each semicircle corresponds to one Debye relaxation process [23]. This is shown in figure 8a, the dependence of ε'' from ε' for prepared composite samples measured in the 8–12 GHz frequency interval. The curve of ε'versus ε'' shows that BNKT/ paraffin wax has a clear segment of three semicircles, demonstrating that the composites have multi-dielectric relaxation processes, representing the contribution of the Debye relaxation process to the enhanced dielectric properties of BNKT.

It is known that the magnetic loss due to eddy currents at a given frequency can be calculated by the formula (3) [24]:

$$C_0 = \frac{\mu''}{\mu'^2.f} \tag{3}$$

where f is the frequency. The calculation results for the composite samples in the frequency range of 8–12 GHz are presented in figure 8b. It can be seen that C_0 slightly changed with increase of frequency, its value fluctuate around a certain mean value. This means that in the BNKT/ paraffin wax, there is a little dependence of eddy currents on the frequency.

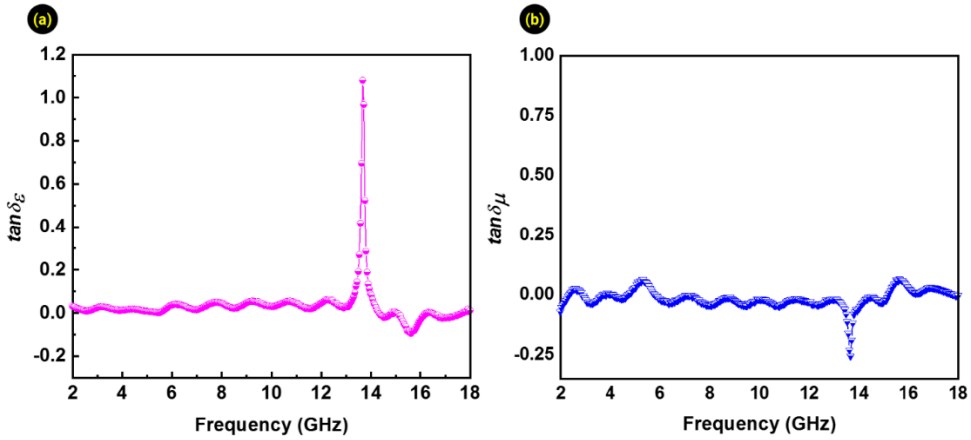

Figure 9. The dielectric loss coefficient $tan\delta_\varepsilon$ (a), magnetic loss $tan\delta_\mu$ (b) of BNKT/paraffin wax measured in frequency range from 2-18 GHz.

Dielectric and magnetic dissipation factors $tan\delta = \varepsilon''/\varepsilon'$ and $tan\delta_\mu = \mu''/\mu'$ provide a measure of the amount of power lost in a material with respect the amount stored [25-27]. The dependence of $tan\delta_\varepsilon$ and $tan\delta_\mu$ on the frequency of BNKT/ paraffin wax composite samples of 50% mass ratio and 3.2 mm thickness in the frequency range from 2-18GHz (Figure 9). In general, the large absorption of radar waves depends on magnetic, dielectric, or both waves [28]. As shown in figure 9a, the $tan\delta_\varepsilon$ value has a single peak at 13.66 GHz and reaches a value of 1.07. On the other hand, the dielectric loss is almost negligible and is approximately zero at other frequencies. This is also observed in figure 9b,

corresponding to the frequency value of 13.66 GHz, the $tan\delta_\mu$ value drops to -0.24. This result represents the change in the real value.

According to the wave propagation theory, the reflection loss (RL) path depends on the sample thickness [29]. The thickness affects the intensity and position of the RL peaks. The change of RL with frequency for the BNKT/ paraffin wax sample (mass ratio 50%) with different thicknesses is shown in figure 10. It can be seen that with a sample thickness of 1.6 mm, the maximum RL value of the sample is about -6.4 dB at 15.62 GHz, which is more than -10 dB in magnitude. However, all samples with larger thicknesses have a maximum RL value less than -10 dB. For the samples with the thickness is 2.6, 2.8 and 4.0 mm, the values of the maximum reflected loss are of -13.22, -20.02 and -19.57 dB, respectively.

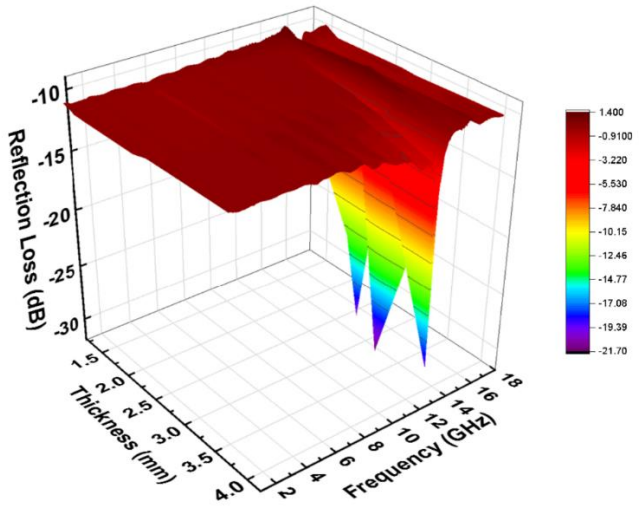

Figure 10. Reflection loss of BNKT/ paraffin wax samples with different thicknesses (1.6 - 4.0 mm) in the frequency range from 2-18 GHz.

Table 2. Microwave absorbing materials performance of composite materials reported in other literatures.

Nanomaterial	Matrix	Filing ratio (wt.%)	d (mm)	Max RL (dB)	Freq (GHz)	Year	Ref
$BaTiO_3$	polyaniline	25	3	- 15	10	2005	[29]
$BaTiO_3$ (nanotube)	Parrafin wax	40	2	- 4.7	15	2012	[30]
$BaTiO_3$ (nanotube)	Parrafin wax	50	2	- 7.0	15	2012	[30]
$BaTiO_3$ (nanotube)	Parrafin wax	60	2	- 16.9	15	2012	[30]
$BaTiO_3$ (nanotube)	Parrafin wax	70	2	- 21.8	15	2012	[30]
$BaTiO_3$ nanoparticales	Parrafin wax	60	2	-21.1	18	2015	[19]
$BaTiO_3$	Epoxy	15	3	- 6.5	12.3	2017	[31]
$BaTiO_3$	Epoxy	15	4	- 11.66	10.88	2017	[31]
$BaTiO_3$	Epoxy	15	5	- 12.85	8.60	2017	[31]
$BaTiO_3$	--	100	12	- 13.33	10.04	2020	[32]
$Bi_{0.5}(Na,K)_{0.5}TiO_3$	Parrafin wax	50	3.2	-21.72	13.66	2021	This work

Especially with a thickness of 3.2 mm, the BNKT/ paraffin wax composite sample gives a maximum absorption coefficient RL of -21.72 dB (99.9%) at 13.66 GHz. It can be concluded that with a certain

thickness, the RL of the composite sample has enhanced absorption intensity peak and this peak has moved to the low frequency range. Thus, it is possible to prepare composite samples with an optimal thickness for the best absorption of the radar waves. However, increasing the thickness too much will affect the impedance of the materials, resulting in the reduce of the ability to absorb electromagnetic waves as well as material consumption. Therefore, the absorption layer thickness always must satisfy the phase condition or the shift-length effect. Lead-free BNKT has a microwave absorbing performance (-21.72 dB) better than the $BaTiO_3$ nanostructures, typical ferroelectric materials as reported in [19, 29-32]. The microwave absorption properties of some representative microwave absorption materials are listed in Table 2.

4. Conclusion

In this work, we have successfully fabricated lead-free BNKT dielectric materials with particle size below 400 nm by using sol-gel method. The crystalline structure of the samples exhibit a single phasewith a good chemical stoichiometry, without impurities. The fabricated materials have weak ferromagnetic properties with saturation magnetism at 5 kOe magnetic field of $26.70.10^{-3}$ emu/g, residual magnetism of and $1.36.10^{-3}$ emu/g, and coercivity of 59.42 Oe. In addition, the dielectric constant is large in the frequency range of 100 Hz - 4MHz.This is typical ferroelectric properties with residual polarization and reactance are 0.34 μC/cm^2 and 910 V/cm respectively at electric field 1kV/cm. Investigation of the absorption of electromagnetic waves of BNKT/paraffin wax composites (with the mass ratio of 50%) has showed that the absorption of the electromagnetic waves has reached a value as large as 99.9% (-21.72 dB) at frequency of 13.66 GHz for 3.2 mm-thicked samples. The results of the investigation of the change in the dielectric constant and magnetic permeability vs. frequency showed that the enhancement in the absorption of electromagnetic wave in the composite materials can be explained due to the appropriate combination between dielectric and magnetic loss.

Acknowledgments

This work has been supported by the VNU University of Engineering and Technology under Project number CN20.06. Nguyen Dang Co was funded by Vingroup JSC and supported by the Master, PhD Scholarship Programme of Vingroup Innovation Foundation (VINIF), Institute of Big Data, code VINIF.2021.TS.005.

References

[1] Y. Liu, Z. Chen, W. Xie, S. Song, Y. Zhang, L. Dong, In-Situ Growth and Graphitization Synthesis of Porous Fe_3O_4/Carbon Fiber Composites Derived from Biomass as Lightweight Microwave Absorber, ACS Sustainable Chem. Eng., Vol. 7, No. 5, 2019, pp. 5318-5328, https://doi.org/10.1021/acssuschemeng.8b06339.

[2] M. Qiao, X. Lei, Y. Ma, L. Tian, K. Su, Q. Zhang, Dependency of Tunable Microwave Absorption Performance on Morphology-Controlled Hierarchical Shells for Coreshell Fe_3O_4@ MnO_2 Composite Microspheres, Chem. Eng. J., Vol. 304, No. 15, 2016, pp. 552-562, https://doi.org/10.1016/j.cej.2016.06.094.

[3] S. Wei, X. Wang, B. Zhang, M. Yu, Y. Zheng, Y. Wang, J. Liu, Preparation of Hierarchical Core-Shell C@$NiCO_2O_4$@Fe_3O_4 Composites for Enhanced Microwave Absorption Performance, Chem. Eng. J., Vol. 314, No. 15, 2017, pp. 477-487, https://doi.org/10.1016/j.cej.2016.12.005.

[4] Y. Akinay, F. Hayat, Synthesis and Microwave Absorption Enhancement of $BaTiO_3$ Nanoparticle/ Polyvinylbutyral Composites, J. Compos. Mater., Vol. 53, No. 5, 2018, pp. 593-601, https://doi.org/10.1177/0021998318788144.

[5] R. C. Che, C. Y. Zhi, C. Y. Liang, X. G. Zhou, Fabrication and Microwave Absorption of Carbon Nanotubes/$CoFe_2O_4$ Spinel Nanocomposite, Appl. Phys. Lett., Vol. 88, No. 3, 2006, pp. 033105, https://doi.org/10.1063/1.2165276.

[6] J. Hongxia, L. Qiaoling, Y. Yun, G. Zhiwu, Y. Xiaofeng, Preparation and Microwave Adsorption Properties of Core–Shell Structured Barium Titanate/Polyaniline Composite, J. Magn. Magn. Mater., Vol. 332, 2013, pp. 10-14, https://doi.org/10.1016/j.jmmm.2012.11.010.

[7] N. Zhang, Y. Huang, M. Wang, 3D Ferromagnetic Graphene Nanocomposites with ZnO Nanorods and Fe_3O_4 Nanoparticles Co-Decorated for Efficient Electromagnetic Wave Absorption, Compos. Part. B. Eng., Vol. 136, 2018, pp.135-142, https://doi.org/10.1016/j.compositesb.2017.10.029.

[8] A. Ullah, A. Ullah, I. W. Kim, D. S. Lee, S. J. Jeong, C. W. Ahn, Large Electromechanical Response in Lead-Free La-Doped BNKT–BST Piezoelectric Ceramics, J. Am. Ceram. Soc., Vol. 97, No. 8, 2014, pp. 2471-2478, https://doi.org/10.1111/jace.12952.

[9] P. Y. Chen, C. S. Chen, C. C. Chou, T. Y. Tseng, H. D. Chen, Microstructures and Electrical Properties of Lead-Based PBZNZT and Lead-Free BNKT Piezoelectric Ceramics Using Microwave Sintering, Curr. Appl. Phys., Vol. 11, No. 3, 2011, pp. S110-S119, https://doi.org/10.1016/j.cap.2011.03.039.

[10] A. Sasaki, T. Chiba, Y. Mamiya, E. Otsuki, Dielectric and Piezoelectric Properties of $(Bi_{0.5}Na_{0.5})TiO_3$–$(Bi_{0.5}K_{0.5})TiO_3$ Systems, Jpn. J. Appl. Phys., Vol. 38, No. 9S, 1999, pp. 5564-5567, https://doi.org/10.1143/JJAP.38.5564.

[11] H. Nagata, M. Yoshida, Y. Makiuchi, T. Takenaka, Large Piezoelectric Constant and High Curie Temperature of Lead-Free Piezoelectric Ceramic Ternary System Based on Bismuth Sodium Titanatebismuth Potassium Titanate-Barium Titanate Near the Morphotropic Phase Boundary, Jpn. J. Appl. Phys., Vol. 42, No. 12, 2003, pp. 7401-7403, https://doi.org/10.1143/JJAP.42.7401.

[12] J. E. Camargo, R. Parra, L. A. Ramajo, M. S. Castro, Synthesis and Characterization of $Bi_{0.5}(Na_{0.8}K_{0.2})_{0.5}TiO_3$-Based Ceramics Obtained Through the Sol-Gel Method, Ferroelectrics, Vol. 545, No. 1, 2019, pp. 62-69, https://doi.org/10.1080/00150193.2019.1621712.

[13] P. Chen, S. Wu, P. Li, J. Zhai, B. Shen, The Phase Formation Process of $Bi_{0.5}(Na_{0.8}K_{0.2})_{0.5}TiO_3$ Thin Films Prepared Using the Sol-Gel Method, Ceram. Int., Vol. 44, No. 6, 2018, pp. 6402-6408, https://doi.org/10.1016/j.ceramint.2018.01.034.

[14] J. Camargo, L. Ramajo, F. R. Marcos, M. Castro, Ferroelectric Properties of $Bi_{0.5}(Na_{0.8}K_{0.2})_{0.5}TiO_3$ Ceramics, Adv. Mater. Res., Vol. 975, 2014, pp. 3-8, https://doi.org/10.4028/www.scientific.net/AMR.975.3.

[15] K. Yoshii, Y. Hiruma, H. Nagata, T. Takenaka, Electrical Properties and Depolarization Temperature of $(Bi_{1/2}Na_{1/2})TiO_3$–$(Bi_{1/2}K_{1/2})TiO_3$ Lead-Free Piezoelectric Ceramics, Jpn. J. Appl. Phys., Vol. 45, No. 5B, 2006, pp. 4493-4496, https://doi.org/10.1143/JJAP.45.4493.

[16] National Physical Laboratory, Electrical Insulation Materials, Kaye And Laby Tables of Physical and Chemical Constants, https://web.archive.org/web/20070927004133/http://www.kayelaby.npl.co.uk/general_physics/2_6/2_6_3.html (accessed on: April 20^t, 2021).

[17] G. Wang, Y. Chang, L. Wang, L. Liu, Ch. Liu, Facilely Preparation and Microwave Absorption Properties of Fe_3O_4 Nanoparticles, Mater. Res. Bul., Vol. 48, No. 3, 2013, pp. 1007-1012, https://doi.org/10.1016/j.materresbull.2012.11.089.

[18] Z. Wang, L. Wu, J. Zhou, B. Shen, Z. Jiang, Enhanced Microwave Absorption of Fe_3O_4 Nanocrystals after Heterogeneously Growing with ZnO Nanoshell, RSC Adv., Vol. 3, 2013, pp. 3309-3315 , https://doi.org/10.1039/C2RA23404A.

[19] L. Tian, X. Yan, J. Xu, P. Wallenmeyer, J. Murowchick, L. Liu, X. Chen, Effect of Hydrogenation on the Microwave Absorption Properties of $BaTiO_3$ Nanoparticles, J. Mater. Chem. A., Vol. 3, No. 23, 2015, pp. 12550-12556, https://doi.org/10.1039/C5TA02109J.

[20] N. D. Co, L. V. Cuong, B. D. Tu, P. D. Thang, L. X. Dien, V. N. Hung, N. D. Quan, Effect of Crystallization Temperature on Energy-Storage Density and Efficiency of Lead-Free $Bi_{0.5}(Na_{0.8}K_{0.2})_{0.5}TiO_3$ Thin Films Prepared by Sol-Gel Method, J. Sci. Adv. Mater. Dev., Vol. 4, No. 3, 2019, pp. 370-375, https://doi.org/10.1016/j.jsamd.2019.04.008.

[21] M. Wang, G. Ji, B. Zhang, D. Tang, Y. Yang, Y. Du, Controlled Synthesis and Microwave Absorption Properties of $Ni_{0.6}Zn_{0.4}Fe_2O_4$/PANI Composite Via an In-Situ Polymerization Process, J. Magn. Magn. Mater., Vol. 377, 2015, pp. 52-58, https://doi.org/10.1016/j.jmmm.2014.10.066.

[22] P. Butnoi, S. Manotham, P. Jaita, K. Pengpat, S. Eitssayeam, T. Tunkasiri, G. Rujijanagul, Effects of Processing Parameter on Phase Transition and Electrical Properties of Lead-Free BNKT Piezoelectric Ceramics, Ferroelectrics, Vol. 511, No. 1, 2017, pp. 42-51, https://doi.org/10.1080/00150193.2017.1333364.

[23] B. Wen, M. Cao, M. Lu, W. Cao, H. Shi, J. Liu, X. Wang, H. Jin, X. Fang, W. Wang, J. Yuan, Reduced Graphene Oxides: Light-Weight and High-Efficiency Electromagnetic Interference Shielding at Elevated Temperatures, Adv. Mater., Vol. 26, No. 21, 2014, pp. 3484-3489, https://doi.org/10.1002/adma.201400108.

[24] P. Liu, Y. Huang, X. Zhang, Cubic $NiFe_2O_4$ Particles on Graphene-Polyaniline and Their Enhanced Microwave Absorption Properties, Compos. Sci. Technol., Vol. 107, 2015, pp. 54-60, https://doi.org/10.1016/j.compscitech.2014.11.021.

[25] T. Xia, C. Zhang, N. A. Oyler, X. Chen, Hydrogenated TiO_2 Nanocrystals: A Novel Microwave Absorbing Material, Adv. Mater., Vol. 25, No. 47, 2013, pp. 6905-6910, https://doi.org/10.1002/adma.201303088.

[26] T. Xia, C. Zhang, N. A. Oyler, X. Chen, Enhancing Microwave Absorption of TiO_2 Nanocrystals Via Hydrogenation, J. Mater. Res., Vol. 29, No. 18, 2014, pp. 2198-2210, https://doi.org/10.1557/jmr.2014.227.

[27] M. Khairy, Synthesis, Characterization, Magnetic and Eclectrical Properties of Polyaniline/$NiFe_2O_4$ Nanocomposite, Synth. Metal., Vol. 189, 2014, pp. 34-41, https://doi.org/10.1016/j.synthmet.2013.12.022.

[28] K. Sakai, K. Hiraki, S. Yoshikado, Evaluation of Composite Electromagnetic Wave Absorber Made of Isolated Ni-Zn Ferrite or Permalloy, Electron. Comm. Jpn., Vol. 92, No. 5, 2009, pp. 14-22, https://doi.org/10.1002/ecj.10045.

[29] S. M. Abbas, A. K. Dixit, R. Chatterjee, T. C. Goel, Complex Permittivity and Microwave Absorption Properties of $BaTiO_3$–Polyaniline Composite, Mater. Sci. Eng. B, Vol. 123, No. 2, 2005, pp. 167-171, https://doi.org/10.1016/j.mseb.2005.07.018.

[30] Y. F. Zhu, L. Zhang, T. Natsuki, Y. Q. Fu, Q. Q. Ni, Facile Synthesis of $BaTiO_3$ Nanotubes and Their Microwave Absorption Properties, ACS Appl. Mater. Interfaces., Vol. 4, No. 4, 2012, pp. 2101-2106, https://doi.org/10.1021/am300069x.

[31] Y. Akinay, F. Hayat, Y. Kanbur, H. Gokkaya, S. Polat, Comparison of Microwave Absorption Properties between $BaTiO_3$/Epoxy and $NiFe_2O_4$/Epoxy Composites, Polym. Compos., Vol. 39, No. S4, 2017, pp. E2143-E2148, https://doi.org/10.1002/pc.24497.

[32] Y. B. Zainal, Dedi, A. Manaf, Microstructure and Microwave Absorption Characteristics of $BaTiO_3$-$CoFe_2O_4$ Composites, Key Eng. Mater., Vol. 855, 2020, pp. 322-329, https://doi.org/10.4028/www.scientific.net/KEM.855.322.